Available online at www.sciencedirect.com

ScienceDirect

Ceramics International 39 (2013) 8649–8655

CERAMICS INTERNATIONAL

www.elsevier.com/locate/ceramint

Production of a half cell with a LSM/CGO support for electrochemical flue gas purification

K.B. Andersen*, K.K. Hansen

Department of Energy Conversion and Storage Technical University of Denmark, Frederiksborgvej 399, 4000 Roskilde, Denmark

Received 3 February 2013; received in revised form 11 April 2013; accepted 11 April 2013
Available online 25 April 2013

Abstract

Described herein is the production of a half cell with a strontium-substituted lanthanum manganite/cerium gadolinium oxide support and dense cerium gadolinium oxide electrolyte for electrochemical flue gas purification. The half cells were constructed through tape casting a strontium-substituted lanthanum manganite/cerium gadolinium oxide support and cerium gadolinium oxide electrolyte. The half cells were produced by laminating the support and electrolyte layers followed by sintering. Perfectly flat half cells were constructed with a porous strontium-substituted lanthanum manganite/cerium gadolinium oxide support layer and dense cerium gadolinium oxide electrolyte by adjusting sintering shrinkage at the electrolyte layer and altering the sintering aid.

Keywords: A. Tape casting; CGO; Flue gas purification; LSM

1. Introduction

Nitrogen oxides (NO_x) are formed as a side product at high temperatures during combustion (e.g., of diesel). NO_x is undesirable because it negatively affects human health, which is a serious environmental threat due to acid rain, smog and high local ozone concentrations [1,2].

Therefore, many studies have attempted to remove NO_x from exhaust gasses (e.g., from diesel-fired engines). NO_x can be removed from petrol fired engine exhaust gasses using a three-way catalytic converter. However, due to the excess air used for diesel combustion, the three-way catalytic converter cannot be used to remove NO_x from diesel exhaust gasses. In principle, NO_x can be removed from diesel exhaust gasses using an electrochemical reactor. An electrochemical reactor can include a dense oxide ionic conducting electrolyte layer between two porous electrodes. When a potential is applied across the reactor, NO_x is reduced to nitrogen and oxide ions at the cathode, and the oxide anions are transported through the electrolyte to the anode, where they are oxidised to oxygen [3].

Mixed perovskite-type oxides compose ABO_3 or A_2BO_4. Perovskite-type oxides are typically stable at high temperatures, less expensive (e.g., compared with noble metals) and can have high catalytic activities. The literature has more information on perovskite structure and use [4,5].

A flat asymmetric electrode-supported half-cell with a porous strontium-substituted lanthanum manganite (LSM)/cerium gadolinium oxide (CGO) support and dense CGO electrolyte was constructed. The layers were constructed separately, laminated and then sintered at 1250 °C. The support shrinkage was changed; then, the electrolyte shrinkage was changed. The layers were then co-sintered to produce a flat, adherent anode-supported half-cell. The powder and pore former compositions and level of binder added to the slurries were changed, and the resulting shrinkage was observed.

For the cathode material, LSM and CGO were combined and used because LSM has fair selectivity for NO_x reduction. CGO was used because CGO conducts oxide ions at an acceptable magnitude for the exhaust gas temperature [4].

The electrodes must be porous for the exhaust gas to reach the electrochemical active sites in the electrodes. Pores can be generated by adding pore formers, which burn off during sintering and leave pores in the electrode structure. A previous study showed that graphite is a pore former [6]. It was previously shown that

*Corresponding author. Tel.: +45 4677 5678; fax: +45 4677 5858.
E-mail address: kjan@dtu.dk (K.B. Andersen).

0272-8842/$ - see front matter © 2013 Elsevier Ltd and Techna Group S.r.l. All rights reserved.
http://dx.doi.org/10.1016/j.ceramint.2013.04.043

Table 1
Compositions of the prepared samples.

Sample	LSM (Weight ratio LSM)			CGO type		Graphite size (μm)		PMMA size (μm)	Binder
	1300	1200	800	LSA	ULSA	2.6	10	10	
L1		1	1	X		4.8	11.2		50
L2		1	1		X	4.8	11.2		40
L3		2	1		X	4.8	11.2		40
L4		1	1		X	2.4	5.6		30
L5		1	1		X	3.6	8.4		35
L6		1	1			4.8	11.2		45
L7		1	1	X		4.8		11.2	60
L8	1		1	X		4.8		11.2	60
L9	2		1	X		4.8		11.2	60
L10	4		1	X		4.8		11.2	60

Table 2
Characteristics of the sintered samples.

Sample	Shrinkage (%)	Porosity (%)
L1	27.8	45
L2	23.3	39.4
L3	20.8	41.1
L4	22.3	28.1
L5	22.8	34.2
L6	24.8	35.6
L7	28.6	46.4
L8	26.5	51.8
L9	27.0	44.5
L10	26.8	43.2

PMMA (polymethyl methacrylate) microparticles are promising materials for preparing porous electrodes in solid oxide fuel cells [7–10]. However, PMMA often generates closed pores [11,12]. Thus, a mixture comprising PMMA and graphite was tested for pore formation herein. The hypothesis is that the graphite will interconnect the pores formed by the PMMA microparticles.

2. Experimental

2.1. Suspension and tape preparation

The powders that were used were as follows. For the supports, a mixture comprising $(La_{0.85}Sr_{0.15})_{0.9}MnO_3$ (LSM, Haldor Topsøe A/S, Denmark) and $Ce_{0.9}Gd_{0.1}O_{1.95}$ (CGO, Rhodia, France) at the ratio 65:35 w/w% was used. Before use, the LSM powders were calcined at 800 °C (LSM800, surface area 18 m^2/g), 1200 °C (LSM1200, surface area 1.0 m^2/g) and 1300 °C (LSM1300, surface area 0.1 m^2/g). Two different CGO powder types (CGO-LSA, surface area 12 m^2/g and CGO-ULSA, surface area 7 m^2/g) were also used. To form pores, two different types of graphite (D50 of 2.6 μm (spherical) and D50 of 10 μm (flakes), both Alfa Aesar) and PMMA (Esprix Technologies, MR10G) were used. To construct the electrolyte layers, CGO was used. Co_3O_4 (Alfa Aesar, Germany) or Fe_2O_3 (Alfa Aesar, Germany) was added to the electrolyte tapes to aid sintering.

Table 3
Characteristics of the sintered samples using CGO with 1 w/w% Co_3O_4 as the sintering agent.

Sample	CGO type	Binder excess (%)	Shrinkage (%)
C1	ULSA		21.0
C2	ULSA	10	21.5
C3	LSA		23.5
C4	HSA		25.7
C5	UHSA		30.8

Table 4
Characteristics of the sintered samples using CGO with 1 w/w% Fe_2O_3 as the sintering agent.

Sample	CGO type	Shrinkage (%)
C6	ULSA	22
C7	LSA	24.3
C8	HSA	25.3

Support: Different levels of LSM800, LSM1200 and LSM1300 were mixed and suspended in an azeotropic mixture comprising methylethylketone and ethanol (MEKET) with polyvinylpyrolidone (PVP) as the dispersant. After ball-milling for 2 days, CGO and more PVP were added; the suspension was then milled for additional 24 h. Next, 11.2 w/w% PMMA microparticles or graphite flakes and 4.8 w/w% spherical graphite were added; the suspension was then milled for 5 h. Finally, a mixture comprising a binder, plasticiser and release agent was added, and the suspension was milled overnight. The suspension was tape-casted using a doctor blade adjusted to 1 mm with a 20 cm/min casting speed.

Electrolyte: CGO, Co_3O_4 or Fe_2O_3, MEKET and PVP were mixed, and the suspension was milled for additional 72 h. Finally, a mixture comprising a binder, plasticiser and release agent was added, and the suspension was milled overnight. In addition to CGO-LSA and CGO-ULSA, CGO-HSA (surface area 22 m^2/g) and CGO-UHSA (surface area 35 m^2/g) were used in the electrolyte tapes. When the tapes were dry, the support layer was laminated with the electrolyte layer using the

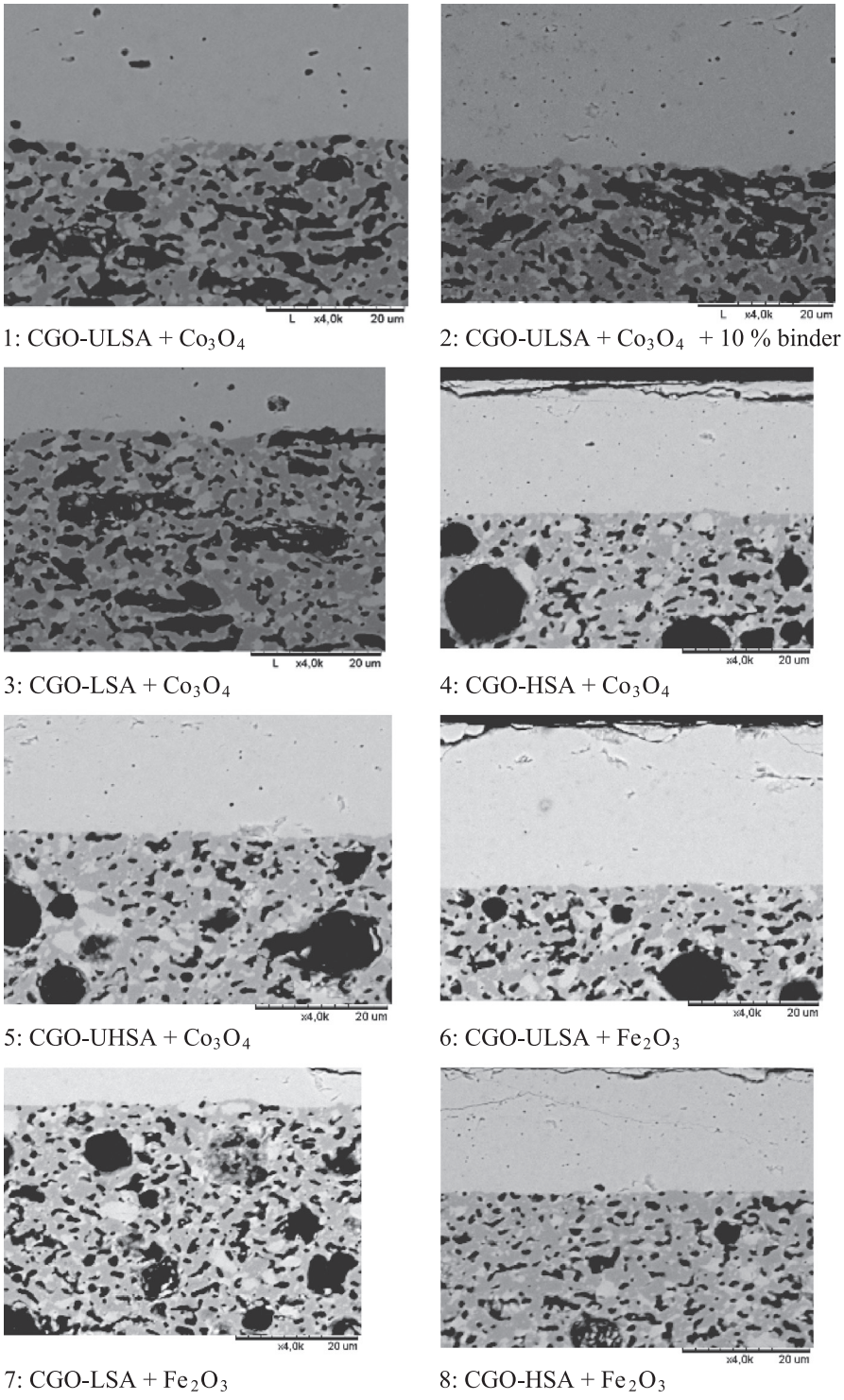

Fig. 1. Micrographs of the sintered CGO electrolytes with support L1 and magnification 5000 times.

method described by Larsen and Brodersen [13]. After lamination, the samples were sintered at 1250 °C for 4 h in air.

2.2. Characterisation

The particle size distribution (PSD) for the slurries was measured after each step using a laser diffraction particle size analyser (LS13320, Beckman Coulter, USA). The slurry viscosities were measured before tape-casting using a Haake RheoStress 600 rheometer (Thermo-scientific, USA) with a parallel plate configuration and 0.1 mm separation between the plates. The slurries were adjusted to the desired viscosity before tape-casting.

The sample shrinkage during sintering was measured as the dimension change after sintering. The sintered samples' microstructures were examined using a tabletop microscope

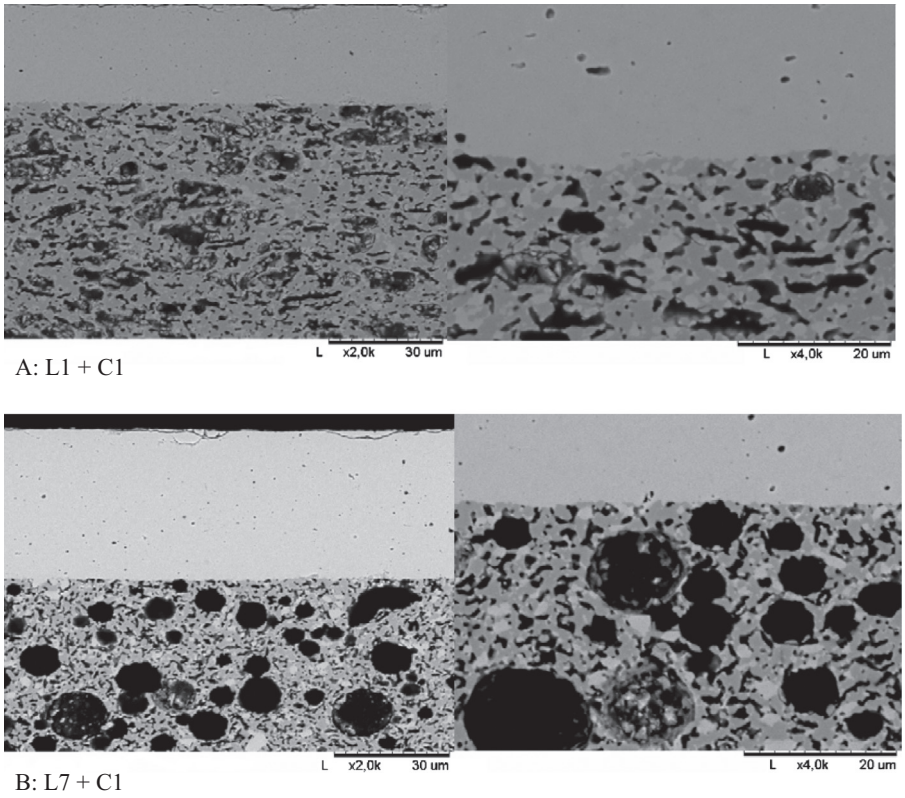

Fig. 2. (A) L1+C1: magnification 2000 and 4000 times; top, dense CGO and (B) L7+C1: magnification 2000 and 4000 times; top, dense CGO.

(Hitachi TM1000, Japan), and the porosities were measured using mercury porosimetry (AutoPore IV, Micromeritics, USA).

Dilatometry was performed using a NETZSCH DIL 402C instrument.

To test for leaks, ethanol was used. One drop of ethanol was applied to the electrolyte layer of the half-cell, and the electrolyte was visually inspected for leaks.

3. Results and discussion

3.1. Support

Table 1 shows the green support tape compositions. The compositions were altered using different LSM and CGO ratios that were pretreated at different temperatures. Further, the binder and pore former levels and the type of pore former were altered. The pore former was added both in different mixtures and at different levels. Finally, the level of binder solution was varied.

In samples L1–L6, only graphite was used to form pores, whereas the large graphite was replaced with PMMA for samples L7–L10. For the samples that only used graphite to form pores, the CGO was added as either CGO-LSA or CGO-ULSA, or no CGO was added. LSM1200 and LSM800 were added at the ratio 1:1 or 2:1. The level of binder was 30–50 g per 100 g of powder. When 10 μm graphite was replaced with PMMA, LSM1300 was also added.

Table 2 shows the sintering shrinkage and porosities after sintering for the samples.

Note that this is not a study in shrinkage behaviour. The different shrinkages for the different supports were measured to determine whether support shrinkage is a central factor in producing flat asymmetric cells with dense electrolyte and porous support. In this work, the support shrinkage was between 21% and 28%.

The support with LSM1200:LSM800 at the ratio 1:1 using CGO-LSA and only graphite to form pores (formulation L1 in Table 1) had 27.8% shrinkage and 45% porosity. By changing the CGO-LSA to CGO-ULSA or removing the CGO, shrinkage decreased. The change in CGO type produced 23.3% shrinkage and 39.4% porosity. Removing CGO from the support generated 24.8% shrinkage and 35.6% porosity. Another method for reducing support shrinkage is reducing the level of graphite. Reducing graphite by 25% and 50% produced 22.8% shrinkage and 34.2% porosity or 22.3% shrinkage and 28.1% porosity, respectively. Further, the LSM ratio can be altered to minimise shrinkage. Using LSM1200:LSM800 at a 2:1 ratio with CGO-LSA generated 20.8% sintering shrinkage and 41.1% porosity.

Using PMMA to form pores generated shrinkage that was not influenced by changes in the LSM and CGO levels. The porosity values are not significantly different. It should be noted that adding LSM1300 produced significantly weaker samples.

3.2. Electrolyte

Table 3 shows the shrinkage change as the type of CGO (increasing the surface area) was varied with 1 w/w% Co_3O_4 as

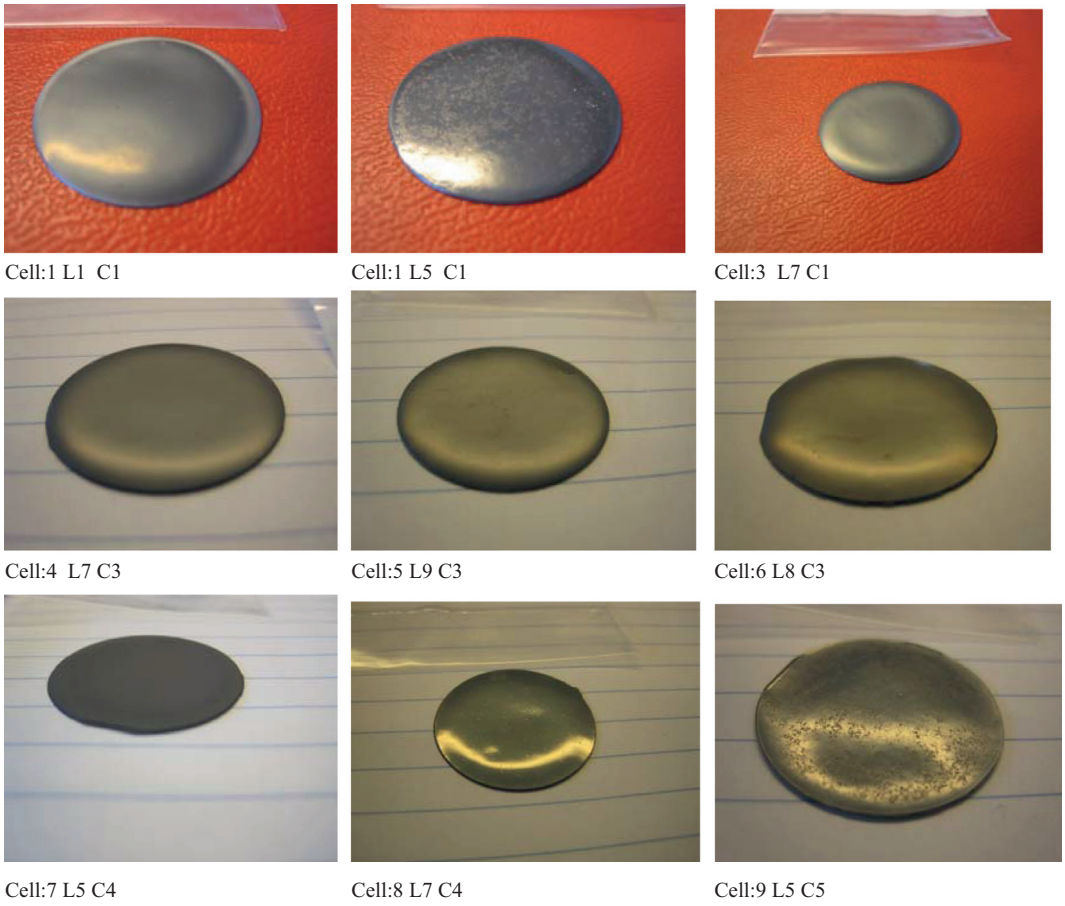

Fig. 3. Asymmetric cell samples pictures using CGO with 1 w/w% Co_3O_4 as the sintering agent. L is the support, and C is the electrolyte. The number refers to the numbers in the above tables.

the sintering agent. CGO-ULSA generated 21% shrinkage. Extra binder solution did not significantly change shrinkage, but handling and sintering was more difficult with the extra binder. When CGO-LSA was used, shrinkage increased to 23.5%; with CGO-HAS, shrinkage was 25.7%; and when CGO-UHSA was used, shrinkage was 30.8%. Table 4 shows the characteristics of the sintered samples with CGO and 1 w/w% Fe_2O_3 as the sintering agent. The shrinkage changed when 1 w/w % Fe_2O_3 was the sintering agent instead of 1 w/w% Co_3O_4. For CGO-ULSA and CGO-LSA, the shrinkage was slightly higher, whereas the shrinkage for CGO-HSA was slightly lower. To conclude, shrinkage primarily depends on the CGO type and less on the level of binder (in the castable range) or the particular sintering agent used.

Fig. 1 shows the different structures generated from different CGO types. CGO-ULSA, CGO-LSA and CGO-HSA were dense on the micrographs, whereas some porosity was observed for the electrolyte with CGO-UHSA, which was also true for samples with Co_3O_4 or Fe_2O_3 as the sintering agent.

3.3. Half cells

Fig. 2 shows the interface region between the support and electrolyte in the asymmetric half-cell. The upper portion (A) is a support where only graphite was used to form pores (L1); the lower portion is a support with graphite and PMMA as the pore formers (L7). The micrographs show different microstructures for the different supports. CGO shows good support adherence with or without PMMA. There is no indication of delamination between the two layers, and in both cases, when CGO is on the support surface, the electrolyte sinters well with the support. The conclusion from Fig. 2 is that adhesion between the electrolyte and support is independent of the pore former used.

3.4. Curvature results

3.4.1. With Co

Fig. 3 shows the sintered half cells produced when Co_3O_4 was used as a sintering agent. The figure shows representative samples for each half cell. The first row shows half cells with an electrolyte generated using CGO-ULSA. When using supports with graphite as the pore former, the cells have almost an arc shape. When using PMMA, the cell shows substantial curvature, but it is a more wave-like structure.

The second row shows half cells with CGO-LSA in the electrolyte. The cells have significant curvature, but the centre is more flat. The curvature is more of an edge curvature. In the last row, the first half cell is with a CGO-HSA electrolyte and a support with only graphite; the second half cell is with a CGO-HSA electrolyte and a support with only PMMA; and the third

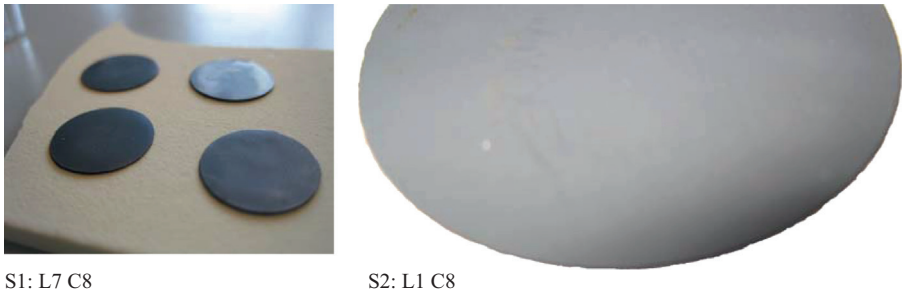

S1: L7 C8 S2: L1 C8

Fig. 4. Sintered asymmetric cells with the CGO-HSA electrolyte, 1 w/w% Fe_2O_3 as the sintering agent and supports with PMMA (S1) and without PMMA (S2).

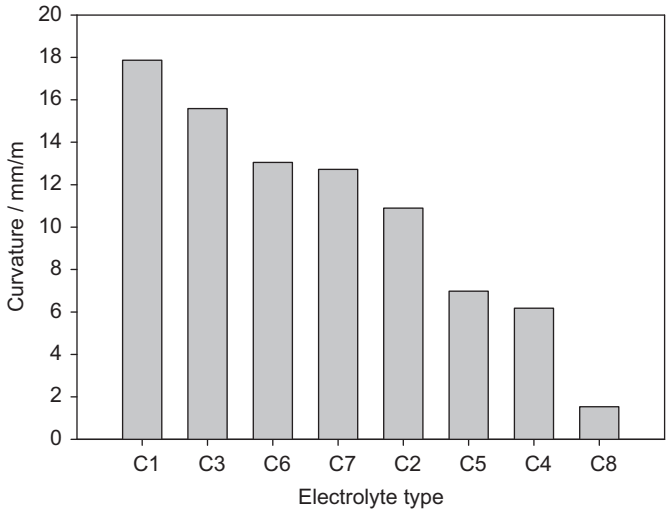

Fig. 5. Curvature of the half cells as a function of electrolyte type.

half-cell is with a CGO-UHSA electrolyte and a support with only graphite. The edge curvature disappeared, but the cells maintain the wave-like structure. All the cells generated are not shown in the table, but a common characteristic is that the half cells are not flat.

Further, each half cell was tested for electrolyte leaks. Cells with electrolyte produced using CGO- ULSA, CHO-LSA and CGO-HSA were leak-proof, whereas half cells with electrolytes comprising CGO-UHSA were not leak-proof.

3.4.2. With Fe

To produce flatter cells, Co_3O_4 was replaced with Fe_2O_3 as a sintering agent. CGO-HSA was the most promising electrolyte in the previous experiments. We generated half cells with both L1 and L7 because we wanted to produce a support that shrinks more than the electrolyte. Fig. 4 shows half cells constructed using the two supports, the CGO-HSA electrolyte and Fe_2O_3 as a sintering agent. The figure shows that the half cells are flat.

To test whether only the change in sintering agent facilitates cell flattening, CGO-ULSA and CGO-LSA were tested using L7. Both types produced edge curling.

The cells were leak-proof as demonstrated using the ethanol test.

Fig. 5 shows the half-cell curvature a function of the electrolyte type. The different supports were laminated to the different electrolytes. Curvature is controlled by the type of electrolyte tape. Therefore, the figure shows curvature as a function of the type of electrolyte tape. The figure shows a strong relationship between curvature and the type of electrolyte. The CGO particle size is essential. The CGO with the largest particle size, C1 (CGO-ULSA), produced the most curvature. When Co_3O_4 was added, the curvature was 17.9 mm/m sample. By changing the tape to C3 (CGO-LSA), the curvature decreased to 15.6 mm/m. When using C4 (CGO-HSA) or C5 (CGO-UHSA), the curvature was almost the same (6.2 and 7.0 mm/m). Adding excess binder (10%) with the CGO-ULSA (C2) as the electrolyte tape, the curvature was 11.0 mm/m, but this produced problems during sintering. Instead, Co_3O_4 was replaced with Fe_2O_3 as the sintering agent, which also yielded a lower curvature. With Fe_2O_3, the curvature was 13.1 mm/m for C6 (CGO-ULSA), 12.7 mm/m for C7 (CGO-LSA) and 1.5 mm/m for C8 (CGO-HSA). Because the asymmetric cells with CGO-UHSA tended to produce a porous electrolyte, this type of tape was not tested with Fe_2O_3. Therefore, the half cells generated using the C8 electrolyte tape had the lowest curvature independent of the support used.

3.5. Dilatometry

The asymmetric cell shape depends on the sintering agent. To study the differences in the two sintering aids used, dilatometry was performed for CGO with 1 w/w% Co_3O_4 or Fe_2O_3 as the sintering agent. Fig. 6 shows the results from this analysis. The dashed line is CGO with 1 w/w% Co_3O_4, and the solid line is CGO with 1 w/w% Fe_2O_3. The figure clearly shows that sintering with Co_3O_4 begins at 800 °C, but with Fe_2O_3, sintering beings at 900 °C. The sequence of CGO behaviour likely influences the sintered half-cell shape. The lower temperature at the beginning of shrinkage for CGO with Co_3O_4 compared with Fe_2O_3 is a likely explanation for the different behaviours. The asymmetric half cells with Co_3O_4 yields curved cells despite the support shrinkage differences. When using Fe_2O_3 as a sintering agent, flat cells may be produced for CGO-HSA and support formulations L1 or L7. Thus, flat cells can be produced with and without PMMA. We could only produce flat half cells with CGO-HSA, not the other types of CGO.

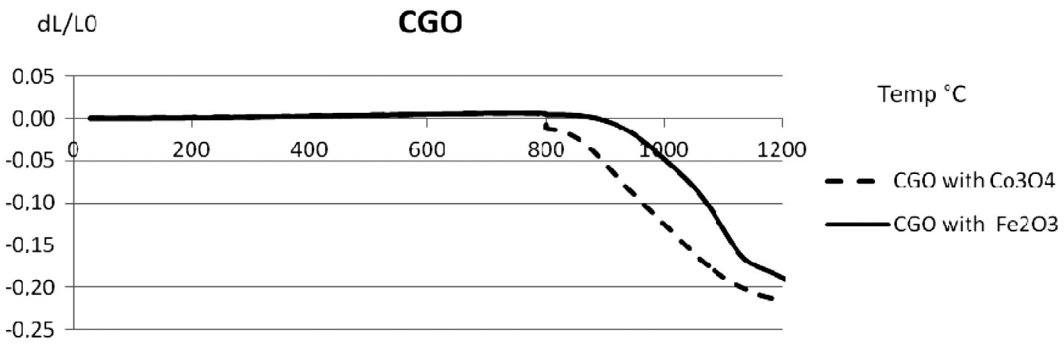

Fig. 6. Dilatometry of CGO with 1 w/w% Co_3O_4 or Fe_2O_3 as the sintering agent.

4. Conclusion

Herein, we describe production of a half cell with a strontium substituted lanthanum manganite/cerium gadolinium oxide support and cerium-based electrolyte for electrochemical removal of NO_x. The half cells were generated through tape-casting a strontium-substituted lanthanum manganite/cerium gadolinium oxide support and cerium gadolinium oxide electrolyte. The half cells were produced by laminating the support and electrolyte layers followed by sintering.

A flat asymmetric half-cell can be generated using a support with strontium-substituted lanthanum manganite calcined at 800 °C and strontium-substituted lanthanum manganite calcined at 1200 °C at the ratio 1:1; using CGO-LSA and 16 w/w% pore former with graphite or strontium-substituted lanthanum manganite calcined at 800 °C and strontium-substituted lanthanum manganite calcined at 1200 °C at the ratio 1:1; and using CGO-LSA, 16 w/w% pore former (4.8 w/w% graphite and 11.2 w/w% polymethyl methacrylate) and the CGO-HSA electrolyte with 1 w/w% Fe_2O_3 as the sintering agent.

References

[1] A.R. Butler, D.L.H. Williams, The physiological-role of nitric-oxide, Chemical Society Reviews 22 (1993) 233.
[2] S.E. Manahan, Environmental Chemistry, sixth ed., CRC, London, 1994.
[3] E.D. Wachsman, P. Jayaweera, G. Krishnan, et al., Electrocatalytic reduction of NO_x on $La_{1-x}A_xB_{1-y}B_yO_{3-d}$: evidence of electrically enhanced activity, Solid State Ionics 136 (2000) 775.
[4] K.K. Hansen, E.M. Skou, H. Christensen, Perovskites as cathodes for nitric oxide reduction, Journal of the Electrochemical Society 147 (2000) 2007.
[5] J. Zhu, A. Thomas, Perovskite-type mixed oxides as catalytic material for NO removal, Applied Catalysis B:Environmental 92 (2009) 225.
[6] K.B. Andersen, F.B. Nygaard, Z. He, et al., Optimizing the performance of porous electrochemical cells for flue gas purification using the DOE method, Ceramics International 37 (2011) 903.
[7] J.C. Ruiz-Morales, J. Canales-Vazquez, J. Pena-Martinez, et al., Micro-structural optimisation of materials for SOFC applications using PMMA microspheres, Journal of Materials Chemistry 16 (2006) 540.
[8] Mingyi Liu, Bo Yu, Jingming Xu, et al., Influence of pore formers on physical properties and microstructures of supporting cathodes of solid oxide electrolysis cells, International Journal of Hydrogen Energy 35 (2010) 2670.
[9] D. Marrero-Lopez, J.C. Ruiz-Morales, J. Pena-Martinez, et al., Preparation of thin layer materials with macroporous microstructure for SOFC applications, Journal of Solid State Chemistry 181 (2008) 685.
[10] J. Carlos Ruiz-Morales, J. Canales-Vazquez, J. Pena-Martinez, et al., On the simultaneous use of La0.75Sr0.25Cr0.5Mn0.5O3-delta as both anode and cathode material with improved microstructure in solid oxide fuel cells, Electrochimica Acta 52 (2006) 278.
[11] M. Descamps, T. Duhoo, F. Monchau, et al., Manufacture of macro-porous beta-tricalcium phosphate bioceramics, Journal of the European Ceramic Society 28 (2008) 149.
[12] H.S. Cruz, J. Spino, G. Grathwohl, Nanocrystalline ZrO_2 ceramics with idealized macropores, Journal of the European Ceramic Society 28 (2008) 1783.
[13] P.H. Larsen, K. Brodersen, Method for the Manufacture of Reversible Solid Oxide Cells, Patent no. US2008124602-A1, 2008.